Letter

Insulator to metal transition by bandwidth reduction

Guoren Zhang [1] and Eva Pavarini [2]
[1] *School of Physics and Technology, Nantong University, Nantong 226019, People's Republic of China*
[2] *Peter Grünberg Institute, Forschungszentrum Jülich, D-52425 Jülich, Germany*

(Received 27 March 2025; accepted 17 October 2025; published 4 November 2025)

In a classic Mott system, the transition from the insulating to the metallic state occurs when the lattice spacing is reduced such that the increase in bandwidth W overcomes the local Coulomb repulsion U. In this picture, both W and the ratio W/U become larger with decreasing the distance between correlated sites. Here we show that, in transition-metal compounds, there is another path to metallization. It is associated with an expansion (instead of a compression) of the lattice and thus with a *decrease* in W. In this scenario W/U grows with increasing distance—the opposite of the classical Mott case. Such a surprising inversion can be obtained by decoupling the main factors controlling W and screening. This mechanism explains the electronic behavior of the t_{2g}^2 triangular lattice series $LiVX_2$ (X = O, S, and Se) with increasing anionic size.

DOI: 10.1103/m3r6-ylxr

Introduction. The insulator to metal transition (IMT) occurs when the bandwidth of correlated electrons, W, increases beyond a critical value, overcoming the local Coulomb repulsion U. In the classical Mott picture, W decreases with increasing lattice spacing, and the ratio W/U follows; the metallic state thus emerges by lattice compression [1]. This scenario is believed to apply to most correlated transition-metal compounds (TMCs). In real materials, complexity arises because of multiorbital effects. The latter take place within the correlated-electrons space and have various causes: orbital degeneracy and its reduction, the Hund's rule coupling, the crystal-field splitting, the spin-orbit coupling, and the subtle interplay of all that [2–9]. This does not change the overall picture, however. The reason is that W and U are typically controlled via the same effects—e.g., the hybridization with the anionic p states—but W is more sensitive than screening to lattice changes. The metallic phase is thus expected to be stabilized by lattice compression.

Here we show that, surprisingly, there is an alternative path to the IMT, which goes via lattice *expansion*. This requires that the main factors controlling bandwidth and screening are decoupled. The picture is illustrated in Fig. 1 in a possible realization. In TMCs, lattice expansion eventually leads to a decrease of W, everything else staying the same. There are different ways of expanding the lattice, however. A possible path is the chemical substitution of the anions with larger ions in the same group ($2p \rightarrow 4p$). This choice, in specific structures, can indeed disentangle bandwidth and screening. In this situation, while W itself decreases, screening becomes rapidly more effective. Under certain circumstances, one can then reach a paradoxical situation: by expanding the lattice, while W decreases, the ratio W/U increases, and the system turns metallic (inverse Mott transition).

This mechanism explains the puzzling trends in the electronic properties of the t_{2g}^2 $LiVX_2$ series (X = O, S, and Se). These materials have attracted attention because of the unusual formation of complex molecular clusters and valence-bond solid (VBS) states at low temperature [10–25]. The

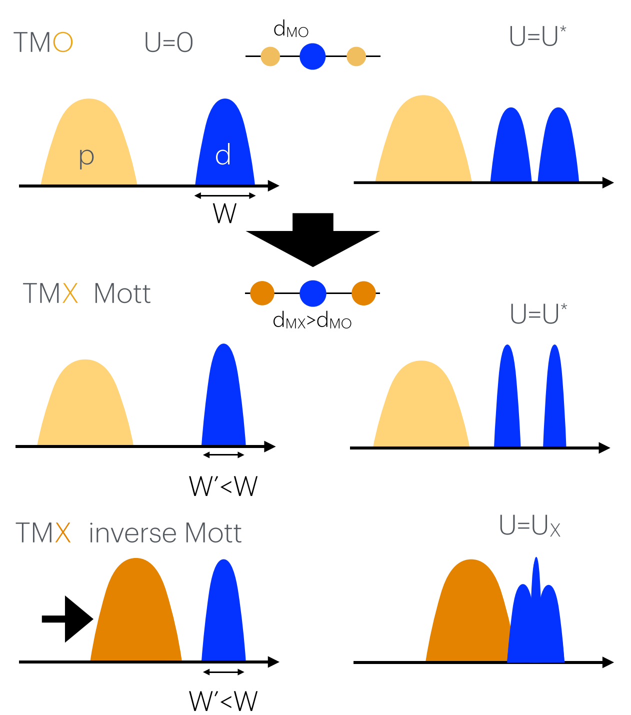

FIG. 1. Insulator to metal transition by lattice expansion. Top: Spectral functions of an insulating transition-metal oxide, for $U = 0$ (left) and for a U sufficiently large to open a gap (right). Correlated bands: blue. Anion bands: orange. Center: O is replaced by a larger anion X and the lattice spacing increases; the bandwidth W (left) is reduced. In a classic Mott picture, this enlarges the gap (right). Bottom: As in the central panel, but, in addition, the distance between anionic and correlated bands decreases (left), making screening more efficient. This eventually leads to metallization (right).

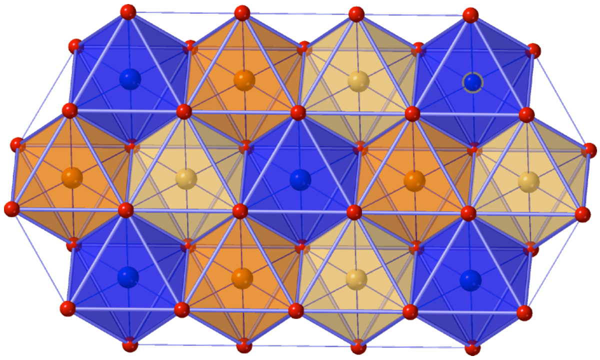

FIG. 2. Part of a VO_6 layer in $LiVO_2$. Layers are made by edge-sharing VO_6 octahedra forming a triangular lattice (O: red spheres; V: remaining spheres); they are divided by triangular Li lattices, not shown.

crystal structure is made by layers of edge-sharing VX_6 octahedra, separated by Li atoms forming themselves a triangular lattice. The V t_{2g} bands crossing the Fermi level are narrow and the systems are correlated. Experimentally, $LiVO_2$ is a small gap insulator; from resistivity measurements the gap is 0.1–0.2 eV [26,27]. The system exhibits a phase transition to a VBS upon cooling, with critical temperature $T_c \approx 500$ K. Instead, $LiVS_2$ and $LiVSe_2$ are metallic above T_c; more specifically, $LiVS_2$ is a metal down to 300 K and $LiVSe_2$ is a metal down to 2 K [18]. The question we address here is why, for $T > T_c$, an insulator to metal transition is observed by increasing the anion size. In early works, this was seen as a consequence of an increase in W due to chemical pressure [18], hence to a classical Mott mechanism. Here we show that this explanation does not hold, however. Instead, the behavior is well captured by the different path to metallization described in the last panel of Fig. 1.

Theoretical method. We adopt the density functional theory + dynamical mean-field theory (DFT + DMFT) approach to construct and solve the t_{2g} Hubbard model describing the correlated V bands close to the Fermi level [28–30]. The noninteracting part of the model is obtained from linearized augmented plane-wave band-structure calculations based on the WIEN2K code [31]. From the latter we construct Wannier functions spanning the t_{2g} bands and obtain the associated Hubbard model:

$$\hat{H} = -\sum_{ii'\sigma}\sum_{mm'} t^{i,i'}_{mm'} c^{\dagger}_{im\sigma} c_{i'm'\sigma} + U\sum_{im} \hat{n}_{im\uparrow}\hat{n}_{im\downarrow} + \frac{1}{2}\sum_{i\sigma\sigma'}\sum_{m\neq m'} (U - 2J - J\delta_{\sigma,\sigma'})\hat{n}_{im\sigma}\hat{n}_{im'\sigma'} - J\sum_{im\neq m'} \left(c^{\dagger}_{im\uparrow}c^{\dagger}_{im\downarrow}c_{im'\uparrow}c_{im'\downarrow} + c^{\dagger}_{im\uparrow}c_{im\downarrow}c^{\dagger}_{im'\downarrow}c_{im'\uparrow}\right). \quad (1)$$

Here m and m' are V t_{2g} orbitals and i site indices; the parameters $t^{i,i'}_{mm'}$ are the hopping integrals ($i \neq i'$) or crystal-field matrix elements ($i = i'$). The lattice structure is shown in Fig. 2. The site symmetry at the V site is D_{3d}, so that the t_{2g} states split into an a_{1g} singly degenerate level and an e^{π}_{g} doublet; for ideal regular octahedra, a_{1g}:$\frac{1}{\sqrt{3}}|xy - yz + xz\rangle$ and e^{π}_{g}:$\{\frac{1}{\sqrt{6}}|2xy + yz - xz\rangle, \frac{1}{\sqrt{2}}|yz + xz\rangle\}$. The bare CF splitting

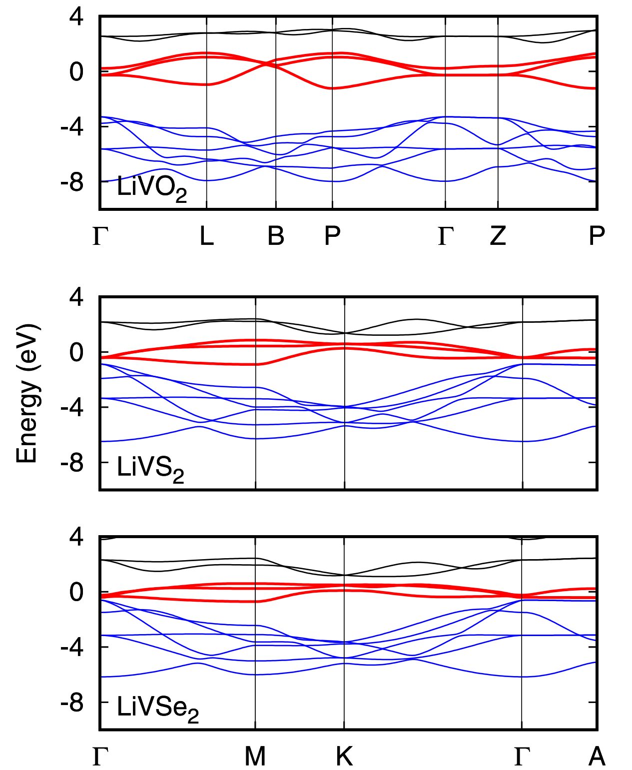

FIG. 3. $LiVX_2$ band structure with increasing anion size. From top to bottom: The t_{2g} bandwidth W (red) decreases, and the anion bands (blue) move closer to the Fermi level.

between a_{1g} and e^{π}_{g} states is $\varepsilon_{CF} = 126$, 104, and 96 meV for X = O, S, and Se, respectively, with the a_{1g} state having higher energy in all cases. We solve the correlated quantum-impurity problem via the weak-coupling continuous-time quantum Monte Carlo method [32], as implemented in Refs. [33–36]. Finally, we calculate the screened Coulomb parameters U and J by the constrained random-phase approximation method [37] via the GAP2 code [38], obtaining $U \approx 4.3$ eV and $J \approx 0.49$ eV for X = O, $U \approx 2.2$ eV and $J \approx 0.38$ eV for X = S, and $U \approx 1.9$ eV and $J \approx 0.36$ eV for X = Se [39]. The experimental crystal structure data for $LiVO_2$, $LiVS_2$, and $LiVSe_2$ are from Refs. [10–12,25]. The average Coulomb repulsion is given by $U_{av} = U - 2J$.

Results. Figure 3 shows the evolution of the band structure when X changes from O to Se. The figure shows that the t_{2g} bandwidth *decreases* from $W \approx 2.64$ eV for X = O to $W \approx 1.82$ eV for X = Se. The origin of the bandwidth reduction can be traced down to the increase of the V-V distance, which strongly suppresses direct V-V hopping integrals. The difference in the staking of layers ($R\bar{3}m$ space group for $LiVO_2$ and $P\bar{3}m1$ for the other two systems) has instead a small role; in fact, an idealized calculation for $LiVO_2$ with the $P\bar{3}m1$ structure even yields a slightly larger $W \approx 2.72$ eV. The reduction of W with increasing anionic size, with everything else staying the same, suggests that $LiVSe_2$ should be more correlated than $LiVO_2$. Intra t_{2g} multiorbital effects, such as the reduction in CF splitting, ε_{CF}, could of course affect this conclusion, however. In fact, a decrease in ε_{CF} can enhance orbital fluctuations, reducing the strength of correlations [8].

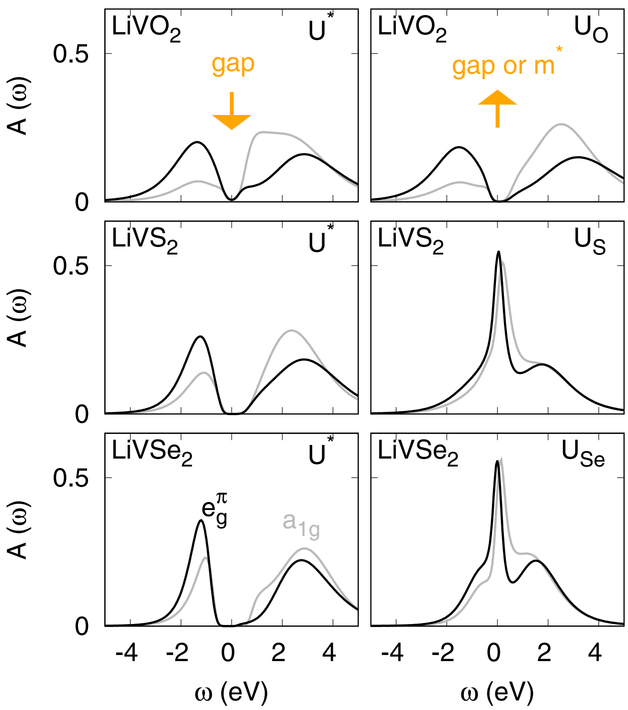

FIG. 4. Spectral functions for constant $U_{\mathrm{av}} = U^*$ (left) and including X-dependent screening (right) [39]. Left column: The gap increases with increasing anionic radius. Right column: The opposite behavior is observed. Calculations are for $\beta = 10\ \mathrm{eV}^{-1}$ (above T_c). Orange arrows: Direction in which the strength of correlation increases in each column.

Furthermore, in the t_{2g}^2 configuration, the Hund's rule coupling can also modify the strength of correlations [4–6], and cRPA calculations show that J decreases (from 0.49 to 0.36 eV) with increasing ionic size. Hence, the metallic behavior could be the result of changes in orbital physics *within* the space of correlated t_{2g} states. This, as we discussed in the Introduction, remains inside the classic Mott picture.

In order to put this hypothesis to the test, we first perform DFT + DMFT calculations with constant $U_{\mathrm{av}} = U^* \approx 4$ eV, using in each case the cRPA J values. The results are shown in Fig. 4, left-hand side. For $LiVO_2$, top left, we obtain an insulating solution with a gap close to the experimental value. Also the other two systems, however, turn out insulators in the calculations; furthermore, the gap increases with increasing the size of the anion. This behavior could arise from suppression of orbital fluctuation, bandwidth reduction, or both combined. To disentangle these effects, we calculate the orbital polarization $p(X) = \frac{1}{2} n_{e_g^\pi} - n_{a_{1g}}$. The latter ranges from $p = -2.0$ [orbital ordering with the $a_{1g}^2(e_g^\pi)^0$ configuration] to $p = 1.0$ [orbital ordering with the $a_{1g}^0(e_g^\pi)^2$ configuration]; strong orbital fluctuations yield $p \approx 0$. Here we find $p(\mathrm{O}) \approx 0.52$, $p(\mathrm{S}) \approx 0.35$ and $p(\mathrm{Se}) \approx 0.28$ for $\beta = 10\ \mathrm{eV}^{-1}$. Everything else being the same, this suggests [2,8] that the correlation strength is weaker for $X = \mathrm{Se}$ than for $X = \mathrm{O}$. Thus, the main cause of the gap increase appears to be the reduction of W. Either way, the conclusion is that, from the classic Mott viewpoint, all $LiVX_2$ systems should be insulators, with the largest gap in $LiVSe_2$ [40].

Next we consider the alternative mechanism illustrated in Fig. 1. To this end, we perform additional DFT + DMFT calculations, but this time taking into account materials-dependent screening effects, as obtained in the cRPA. Remarkably we find an unexpectedly strong decrease in U_{av} with increasing anion size: for $X = \mathrm{Se}$, U_{av} becomes about one half of the $X = \mathrm{O}$ value. The resulting spectral functions are shown in the right-hand column of Fig. 4; one can see that the trends with X are the *opposite* of those obtained in the left-hand column. The effective masses m^* increase going from the bottom to the top of the figure (orange arrow); a gap only opens in the case of $LiVO_2$. This is in line with experimental findings. The last question that remains to be addressed is what reduces U_{av} so drastically, sufficiently to reverse the trend. Our results show that the main cause is the reduction of the charge-transfer energy between anionic p and transition-metal $3d$ bands (Fig. 3), rather than the expansion of the wave functions. In fact, the bare direct Coulomb repulsion U_{bare} decreases from 16.6 to 13.5 eV going from $X = \mathrm{O}$ to $X = \mathrm{Se}$; the ratio between screened and bare Coulomb repulsion, $r_X = U/U^{\mathrm{bare}}$, however, takes the value $r_{\mathrm{O}} = 0.26$ for $LiVO_2$, $r_{\mathrm{S}} = 0.16$ for $LiVS_2$, and $r_{\mathrm{Se}} = 0.14$ for $LiVSe_2$. This is exactly the mechanism described in Fig. 1.

Conclusion and outlook. We have shown that, surprisingly, in correlated TMCs, it is possible to obtain an insulator to metal transition by lattice expansion, i.e., decreasing the bandwidth W—as opposed to the classic Mott picture, in which lattice compression is key, so that the bandwidth increases. This unusual behavior can be realized by decoupling the main factors that control bandwidth and screening. In TMCs this disentanglement can be achieved, e.g., replacing O with larger anions of the same group. We have shown that this mechanism finds a realization in the $LiVX_2$ series. The ideas outlined in this Letter are not confined to these compounds, however; they are likely to be at play in other TMCs, in particular, edge-sharing systems, currently the subject of intense research [41–45], since their structure promotes sizable direct-hopping integrals. The results obtained can also provide guidelines to tune correlations in devices based on these materials, e.g., energy-efficient batteries [46,47] or neuromorphic computers [48].

Acknowledgments. G.Z. acknowledges financial support by the National Natural Science Foundation of China under Grant No. 12074384. The authors acknowledge the Gauss Centre for Supercomputing [49] for providing computing time on the GCS Supercomputer JUWELS at the Jülich Supercomputing Centre. The authors also gratefully acknowledge computing time on JURECA [50] at the Forschungszentrum Jülich.

Data availability. The data that support the findings of this article are not publicly available upon publication because it is not technically feasible and/or the cost of preparing, depositing, and hosting the data would be prohibitive within the terms of this research project. The data are available from the authors upon reasonable request.

[1] N. F. Mott, Metal-insulator transition, Rev. Mod. Phys. **40**, 677 (1968).
[2] E. Pavarini, S. Biermann, A. Poteryaev, A. I. Lichtenstein, A. Georges, and O. K. Andersen, Mott transition and suppression of orbital fluctuations in orthorhombic $3d^1$ perovskites, Phys. Rev. Lett. **92**, 176403 (2004).
[3] E. Pavarini, A. Yamasaki, J. Nuss, and O. K. Andersen, How chemistry controls electron localization in $3d^1$ perovskites: A Wannier-function study, New J. Phys. **7**, 188 (2005).
[4] L. de' Medici, Hund's coupling and its key role in tuning multiorbital correlation, Phys. Rev. B **83**, 205112 (2011).
[5] L. de' Medici, J. Mravlje, and A. Georges, Janus-faced influence of Hund's rule coupling in strongly correlated materials, Phys. Rev. Lett. **107**, 256401 (2011).
[6] A. Georges and G. Kotliar, The Hund-metal path to strong electronic correlations, Phys. Today **77**(4), 46 (2024).
[7] G. Zhang and E. Pavarini, Multiorbital nature of doped Sr_2IrO_4, Phys. Rev. Lett. **131**, 036504 (2023).
[8] N. Samani, G. Zhang, and E. Pavarini, Map of crystal-field effects in correlated layered t_{2g}^n perovskites, Phys. Rev. Lett. **132**, 236505 (2024).
[9] G. Zhang and E. Pavarini, Magnetic superexchange couplings in Sr_2IrO_4, Phys. Rev. B **104**, 125116 (2021).
[10] M. Onoda and T. Inabe, Role of structural change in phase transition in $LiVO_2$, J. Phys. Soc. Jpn. **62**, 2216 (1993).
[11] B. Van Laar and D. J. W. Ijdo, Preparation, crystal structure, and magnetic structure of $LiCrS_2$ and $LiVS_2$, J. Solid State Chem. **3**, 590 (1971).
[12] D. W. Murphy, F. J. Di Salvo, G. W. Hull, Jr., and J. V. Waszczak, Convenient preparation and physical properties of lithium intercalation compounds of group 4B and 5B layered transition metal dichalcogenides, Inorg. Chem. **15**, 17 (1976). The third Se coordinate is not given in this work; we thus obtained it by structural optimization calculations using LDA as the functional.
[13] J. B. Goodenough, *Magnetism and the Chemical Bond* (Interscience and Wiley, New York, 1963).
[14] M. Onoda, T. Naka, and H. Nagaswa, Phase transition and spin dynamics in $LiVO_2$, J. Phys. Soc. Jpn. **60**, 2550 (1991).
[15] K. Imai, H. Swa, M. Koike, M. Hasegawa, and H. Takei, Superstructure analyses on single crystals of $Li_{0.8}VO_2$, J. Solid State Chem. **114**, 184 (1995).
[16] H. F. Pen, L. H. Tjeng, E. Pellegrin, F. M. F. de Groot, G. A. Sawatzky, M. A. van Veenendaal, and C. T. Chen, Phase transition in $LiVO_2$ studied by near-edge x-ray-absorption spectroscopy, Phys. Rev. B **55**, 15500 (1997).
[17] S. Yu Ezhov, V. I. Anisimov, H. F. Pen, D. I. Khomskii, and G. A. Sawatzky, Orbital polarization in $LiVO_2$ and $NaTiO_2$, Europhys. Lett. **44**, 491 (1998).
[18] N. Katayama, M. Uchida, D. Hashizume, S. Niitaka, J. Matsuno, D. Matsumura, Y. Nishihata, J. Mizuki, N. Takeshita, A. Gauzzi, M. Nohara, and H. Takagi, Anomalous metallic state in the vicinity of metal to valence-bond solid insulator transition in $LiVS_2$, Phys. Rev. Lett. **103**, 146405 (2009).
[19] T. Tanaka, Y. Kawasaki, S. Endou, S. Kimura, Y. Ideta, Y. Kishimoto, T. Ohno, N. Katayama, M. Nohara, and H. Takagi, Trimer V^{3+} spin singlet state and pseudo gap in $LiVS_2$ studied by ^{51}V and ^{7}Li nuclear magnetic resonance, J. Phys. Soc. Jpn. **78**, 054709 (2009).
[20] T. Jin-no, Y. Shimizu, M. Itoh, S. Niitaka, and H. Takagi, Orbital reformation with vanadium trimerization in d^2 triangular lattice $LiVO_2$ revealed by ^{51}V NMR, Phys. Rev. B **87**, 075135 (2013).
[21] K. Kojima, N. Katayama, S. Tamura, M. Shiomi, and H. Sawa, Vanadium trimers randomly aligned along the c-axis direction in layered $LiVO_2$, Phys. Rev. B **100**, 235120 (2019).
[22] L. Boehnke, A. I. Lichtenstein, M. I. Katsnelson, and F. Lechermann, Hidden spin-orbital hexagonal ordering induced by strong correlations in $LiVS_2$, Phys. Rev. B **102**, 115118 (2020).
[23] K. Kojima, N. Katayama, Y. Matsuda, M. Shiomi, R. Ishii, and H. Sawa, Short-range order and increased transition temperature in $LiVO_2$ with weakened trimer frustration, Phys. Rev. B **107**, L020101 (2023).
[24] K. Kojima, N. Katayama, K. Sugimoto, N. Hirao, Y. Ohta, and H. Sawa, Zigzag chain order of $LiVSe_2$ developing away from the vanadium trimer phase transition boundary, Phys. Rev. B **108**, 094107 (2023).
[25] N. Katayama, K. Kojima, T. Yamaguchi, S. Hattori, S. Tamura, K. Ohara, S. Kobayashi, K. Sugimoto, Y. Ohta, K. Saitoh, and H. Sawa, Slow dynamics of disordered zigzag chain molecules in layered $LiVS_2$ under electron irradiation, npj Quantum Mater. **6**, 16 (2021).
[26] H. Takei, M. Koike, K. Imai, H. Sawa, H. Kadowaki, and Y. Iye, Growth and properties of Li-deficient lithium vanadium dioxide single crystals, Mater. Res. Bull. **27**, 555 (1992).
[27] W. Tian, M. F. Chisholm, P. G. Khalifah, R. Jin, B. C. Sales, S. E. Nagler, and D. Mandrus, Single crystal growth and characterization of nearly stoichiometric $LiVO_2$, Mater. Res. Bull. **39**, 1319 (2004).
[28] See, e.g., *Dynamical Mean-Field Theory of Correlated Electrons*, edited by E. Pavarini, E. Koch, A. I. Lichtenstein, and D. Vollhardt, Modeling and Simulation Series, Vol. 12 (Forschungszentrum Jülich, Jülich, 2022), and references therein.
[29] See, e.g., E. Pavarini, The LDA+DMFT approach, in *The LDA+DMFT Approach to Strongly Correlated Materials*, edited by E. Pavarini, E. Koch, D. Vollhardt, and A. Lichtenstein, Modeling and Simulation Series, Vol. 1 (Forschungszentrum Jülich, Jülich, 2011).
[30] E. Pavarini, Solving the strong-correlation problem in materials, Riv. Nuovo Cimento **44**, 597 (2021).
[31] P. Blaha, K. Schwarz, G. K. H. Madsen, D. Kvasnicka, and J. Luitz, *WIEN2k, an Augmented Plane Wave Local Orbitals Program for Calculating Crystal Properties* (Technische Universität Wien, Austria, 2001); P. Blaha, K. Schwarz, P. Sorantin, and S. Trickey, Full-potential, linearized augmented plane wave programs for crystalline systems, Comput. Phys. Commun. **59**, 399 (1990).
[32] E. Gull, A. J. Millis, A. I. Lichtenstein, A. N. Rubtsov, M. Troyer, and P. Werner, Continuous-time Monte Carlo methods for quantum impurity models, Rev. Mod. Phys. **83**, 349 (2011).
[33] E. Gorelov, M. Karolak, T. O. Wehling, F. Lechermann, A. I. Lichtenstein, and E. Pavarini, Nature of the Mott transition in Ca_2RuO_4, Phys. Rev. Lett. **104**, 226401 (2010).
[34] G. Zhang, E. Gorelov, E. Sarvestani, and E. Pavarini, Fermi surface of Sr_2RuO_4: Spin-orbit and anisotropic Coulomb interaction effects, Phys. Rev. Lett. **116**, 106402 (2016).

[35] G. Zhang and E. Pavarini, Mott transition, spin-orbit effects, and magnetism in Ca_2RuO_4, Phys. Rev. B **95**, 075145 (2017).

[36] E. Sarvestani, G. Zhang, E. Gorelov, and E. Pavarini, Effective masses, lifetimes, and optical conductivity in Sr_2RuO_4 and $Sr_3Ru_2O_7$: Interplay of spin-orbit, crystal-field, and Coulomb tetragonal tensor interactions, Phys. Rev. B **97**, 085141 (2018).

[37] F. Aryasetiawan, M. Imada, A. Georges, G. Kotliar, S. Biermann, and A. I. Lichtenstein, Frequency-dependent local interactions and low-energy effective models from electronic structure calculations, Phys. Rev. B **70**, 195104 (2004).

[38] H. Jiang and P. Blaha, *GW* with linearized augmented plane waves extended by high-energy local orbitals, Phys. Rev. B **93**, 115203 (2016); H. Jiang, R. I. Gómez-Abal, X. Li, C. Meisenbichler, C. Ambrosch-Draxl, and M. Scheffler, FHI-gap: A GW code based on the all-electron augmented plane wave method, Comput. Phys. Commun. **184**, 348 (2013).

[39] Since the cRPA tends to overestimate screening for the direct Coulomb integral U, in DMFT calculations the actual $U_{\rm av}$ has been multiplied by a factor of 1.3, the same for all systems. The Hund's rule coupling J is kept fixed; this ensures that the gap is correctly reproduced for $LiVO_2$.

[40] We obtain similar results for a five-band model including explicitly the e_g states. This is because the splitting between e_g and t_{2g} bands is large (above 1.5 eV) in all cases, and the total d-band width decreases with $X = \rm O \rightarrow Se$.

[41] B. Huang, G. Clark, E. Navarro-Moratalla, D. R. Klein, Ran Cheng, Kyle L. Seyler, D. Zhong, E. Schmidgall, M. A. McGuire, D. H. Cobden, W. Yao, D. Xiao, P. Jarillo-Herrero, and X. Xu, Layer-dependent ferromagnetism in a van der Waals crystal down to the monolayer limit, Nature (London) **546**, 270 (2017).

[42] J. G. Rau, E. K. -H. Lee, and H.-Y. Kee, Generic spin model for the honeycomb iridates beyond the Kitaev limit, Phys. Rev. Lett. **112**, 077204 (2014).

[43] B. R. Ortiz, P. M. Sarte, A. H. Avidor, A. Hay, E. Kenney, A. I. Kolesnikov, D. M. Pajerowski, A. A. Aczel, K. M. Taddei, C. M. Brown, C. Wang, M. J. Graf, R. Seshadri, L. Balents, and S. D. Wilson, Quantum disordered ground state in the triangular-lattice magnet $NaRuO_2$, Nat. Phys. **19**, 943 (2023).

[44] R. Yadav, R. Ray, M. S. Eldeeb, S. Nishimoto, L. Hozoi, and J. van den Brink, Strong effect of hydrogen order on magnetic Kitaev interactions in $H_3LiIr_2O_6$, Phys. Rev. Lett. **121**, 197203 (2018).

[45] A. Banerjee, C. A. Bridges, J.-Q. Yan, A. A. Aczel, L. Li, M. B. Stone, G. E. Granroth, M. D. Lumsden, Y. Yiu, J. Knolle, S. Bhattacharjee, D. L. Kovrizhin, R. Moessner, D. A. Tennant, D. G. Mandrus, and S. E. Nagler, Proximate Kitaev quantum spin liquid in a honeycomb magnet, Nat. Mater. **15**, 733 (2016).

[46] M. Otoyama, T. Takeuchi, N. Taguchi, K. Kuratani, and H. Sakaebe, Mechanochemical synthesis and electrochemical properties of Li_xVS_y positive electrodes for all-solid-state batteries, ECS Adv. **2**, 010501 (2023).

[47] X. Zhang, Q. He, X. Xu, T. Xiong, Z. Xiao, J. Meng, X. Wang, L. Wu, J. Chen, and L. Mai, Insights into the storage mechanism of layered VS_2 cathode in alkali metal-ion batteries, Adv. Energy Mater. **10**, 1904118 (2020).

[48] A. Hoffmann, S. Ramanathan, J. Grollier, A. D. Kent, M. J. Rozenberg, I. K. Schuller, O. G. Shpyrko, R. C. Dynes, Y. Fainman, A. Frano, E. E. Fullerton, G. Galli, V. Lomakin, S. Ping Ong, A. K. Petford-Long, J. A. Schuller, M. D. Stiles, Y. Takamura, and Y. Zhu, Quantum materials for energy-efficient neuromorphic computing: Opportunities and challenges, APL Mater. **10**, 070904 (2022).

[49] www.gauss-centre.eu.

[50] Jülich Supercomputing Centre. JURECA: Data centric and booster modules implementing the modular supercomputing architecture at Jülich Supercomputing Centre, J. Large-Scale Res. Facil. JLSRF **7**, A182 (2021).